What can satellite embedding fields tell us about shallow coral-reef habitats? A decodability survey of AlphaEarth over the Great Barrier Reef

Adam Cropp [1 2]

[1] College of Science and Engineering, James Cook University, Cairns, Queensland, Australia [2] OSIBOT PTY LTD, Cairns, Queensland, Australia

ORCID: https://orcid.org/0009-0001-6975-6055

Corresponding author: adam.cropp@my.jcu.edu.au

This manuscript is a **non-peer-reviewed preprint submitted to EarthArXiv**. It has not been peer reviewed. It is intended for later publication in a peer-reviewed journal and, at the time of this version, has not yet been submitted to a journal.

Supplementary material (supplement text and tables S1–S16, run ledger):
https://doi.org/10.5281/zenodo.22064963

Code and released decoder coefficients (public reproduction pack):
https://doi.org/10.5281/zenodo.22065301

AlphaEarth embedding-window archive used in the analyses:
https://doi.org/10.5281/zenodo.22065348

Preferred citation for this version: Cropp, A. (2026). What can satellite embedding fields tell us about shallow coral-reef habitats? A decodability survey of AlphaEarth over the Great Barrier Reef. EarthArXiv [preprint DOI once assigned].

What can satellite embedding fields tell us about shallow coral-reef habitats? A decodability survey of AlphaEarth over the Great Barrier Reef

Adam Cropp, College of Science and Engineering, James Cook University, Cairns, Queensland, Australia; and OSIBOT PTY LTD, Cairns, Queensland, Australia.

Abstract

Annual satellite embedding fields compress a year of multi-sensor observation into a 64-dimensional vector per 10 m pixel, globally; whether they retain ecologically meaningful information about the submerged reef benthos is untested. We conducted a registered decodability survey of the AlphaEarth Foundations embedding over shallow (< 10 m) Great Barrier Reef habitats: every candidate output was registered with mechanism, test and pass gate before testing, evaluated under one fixed validation protocol (spatial and temporal holdouts, buffered isolation, baseline ablations, cluster-robust uncertainty), and reported pass or fail. Ground truth comprised 104,668 photo-quadrat images (37 sites, 7 years) at one reef, photo-transects at 67 further reefs in two eras, and independent point-label and map products. Benthic state is broadly decodable with linear read-outs: eight channels pass at one or more of six scales (10–100 m), led by hard coral (held-out rho .73 at 10 m, .80 at 50 m). A persistence control shows this cross-sectional skill largely reflects stable habitat structure, refreshed annually. Six channels replicate on never-trained reefs and across survey eras and methods, and decoded sand agrees with the independently produced Allen Coral Atlas at AUC .96 (sand is itself optically recoverable). Year-over-year change, measured at the single multi-year reef, is decodable only in the two documented bleaching-event years and only at 20–50 m: in the stronger (2024) event the coral-loss axis discriminates ≥ 10-point loss blocks at AUC .83 (cluster CI .69–.92; detection 13–85 % at a 10 % false-alarm budget). Quiet-year change lies below the noise floor of the registered linear protocol at every scale and temporal lag. A post-registration campaign against independent AIMS monitoring archives (184 manta-tow reefs; 306 fixed photo-transect sites, 289 after a coordinate screen) bounds deployment: site-level cover transfers at roughly a third of the agreement between the survey programmes themselves (reef windows, a quarter), but decoded trajectories fail with a directional bias (post-disturbance surfaces read as coral, so apparent gains rank below chance), and reef-mean aggregation resolves ≈ 7-point changes only at locally calibrated reefs. Ground-truth reliability places the decodability ceiling near rho .8: the limit is the signal itself, not the amount of data. Naive cross-validation inflated skill by up to +.28 rho, and annotation-scheme differences between ground-truth programmes exceeded ecological signal; both cautions generalise to any embedding-decoding study. The catalogue, its conditional channels and its documented negatives define what satellite embeddings can and cannot yet contribute to reef monitoring.

Keywords: satellite embeddings; coral reefs; benthic mapping; Great Barrier Reef; change detection; validation

1. Introduction

Coral reefs are changing faster than monitoring programmes can measure them. Mass thermal-stress events now recur at intervals shorter than reef recovery times (Hughes et al., 2017, 2018). The 2024 event alone reversed five years of coral-cover gains on the Great Barrier Reef, with the largest declines in the southern sector (Ceccarelli et al., 2026); at One Tree Island, in the same Capricorn–Bunker sector as this study's core reef, it caused catastrophic bleaching inside one of the marine park's most strictly protected zones (Byrne et al., 2025): protection from local pressures offers no refuge from marine heat.

Management responses depend on knowing where reef condition is changing, at what rate, and in which direction. The in-water monitoring programmes that provide this information are rigorous but sparse: the largest long-term programme on the Great Barrier Reef surveys on the order of a hundred reefs out of roughly three thousand (Sweatman et al., 2011; AIMS, 2025), photo-quadrat programmes resolve benthic composition at fixed sites only, and most of the world's reefs are never surveyed at all. The gap between what monitoring measures and what management needs is a gap in where and how often reefs are observed, which satellite observation is positioned to fill.

Satellite remote sensing of reefs has so far filled it in two specific ways (review: Hedley et al., 2016). Thermal products such as Degree Heating Weeks and the bleaching alerts derived from them (Liu et al., 2014; Skirving et al., 2020) predict stress exposure, but exposure is not outcome: they indicate where bleaching is likely but cannot report what died.

Optical mapping products classify the seafloor, exploiting the separability of coral, algae and sand spectra through shallow water (Hochberg and Atkinson, 2003): the Allen Coral Atlas provides global benthic and geomorphic maps from high-resolution imagery (Lyons et al., 2020; Kennedy et al., 2021; Roelfsema et al., 2021a), grounded by water-column and Sentinel-2 capability assessments (Hedley et al., 2018), and Sentinel-2 and Landsat time series have detected individual bleaching events and multidecadal cover trends at well-studied sites (Yamano and Tamura, 2004; Diederiks et al., 2025, at the same core reef used here); but each such time series is a bespoke per-site product, built per-purpose from raw spectral bands. No operational satellite product currently delivers annual, guild-level, change-capable reef information as a general layer.

A new class of geospatial data product offers a different route. Embedding fields, exemplified by AlphaEarth Foundations (Brown et al., 2025), compress a year of multi-sensor satellite observation (optical, radar and thermal inputs) into a fixed-length vector per 10 m pixel, produced globally and released annually. The embedding is not a thematic map: it is a learned summary of the year's sensor record, trained so the compressed vector can reconstruct its input sensors plus wider environmental sources never received at inference (climate, elevation, land cover; Brown et al., 2025). Whatever information the constituent sensors carry about the shallow seafloor is potentially present in the vector, extractable with a linear read-out (a simple regression) trained against field data. Embedding fields have begun to be exploited on land (Brown et al., 2025; Rahman, 2026); we are aware of no published or preprinted marine-benthos application as of August 2026. Whether a global, general-purpose annual embedding retains ecologically meaningful reef information through a water column, at what scale, and with what failure modes, is an open empirical question.

This paper addresses that question with a survey rather than a single demonstration. We ask, for the shallow (< 10 m) reef habitats of the Great Barrier Reef: what can be decoded from the AlphaEarth embedding field, at what spatial scale, with what reliability, and with what limits? The design commits to three principles. First, *registration*: every candidate output (benthic state channels, year-over-year change channels, summary axes, auxiliary layers) was registered before the confirmatory testing, with its mechanism, test and pass gate fixed in advance (see §2.1 for the exploratory-phase qualification). Second, *one protocol*: every candidate faced the same validation battery, so that surviving channels are comparable and failed channels are interpretable. Third, *negatives are results*: outputs that failed are reported with the same statistical detail as those that passed, because the boundary of decodability is the finding.

The survey yields a catalogue with a two-regime structure. Benthic state is broadly decodable, and most state channels validate on reefs never used in training and across survey eras and methods; year-over-year change is decodable only in event years and only at intermediate scales, a regime boundary we map precisely, test against two independent long-term monitoring archives, and for which we offer a physical reading. Alongside the catalogue, the survey produces methodological results for any study decoding satellite representations against field ecology: quantified cross-validation leakage on spatial data, annotation-scheme effects larger than the ecology, and a measured decomposition of the skill ceiling into ground-truth noise and genuine signal limits. Sections 2–4 present the data and validation protocol, the catalogue and its limits, and the implications for reef monitoring and for embedding fields in marine science.

---

2. Materials and methods

2.1 Study design

The study is a decodability survey with a three-step design applied identically to every candidate output. First, each candidate was *registered* before testing: what the output measures, the mechanism by which an annual embedding could carry it, the test, the pass gate (fixed in advance as cluster-robust $p < 0.01$, detection ≥ 30 % sensitivity at 10 % false-positive rate, or a cluster-bootstrap CI excluding the null, per output type) and the expected outcome. Second, every candidate was *tested* under one fixed validation protocol (§2.6), applied without modification. Third, the full catalogue is *reported*, confirmed to refuted: negatives are published as limits with the same statistical detail as positives.

One qualification applies. The register formalises expectations developed in a prior exploratory phase on the same core site, so the confirmatory re-run is not out-of-sample confirmation of those expectations; its value is subjecting every expectation to one hardened protocol. Independent confirmation comes from tests on data unavailable to the exploratory phase: cross-reef transfer (67 reefs), cross-era transfer (2017/18), and the independent map-product and point-label comparisons.

The study domain is shallow (< 10 m depth) coral-reef habitat of the Great Barrier Reef, Australia. The core training and change-analysis site is Heron Reef (Capricorn–Bunker group, southern GBR); cross-reef validation spans 67 additional reefs in three regional groups (Cairns–Cooktown/Far Northern, Townsville–Whitsunday, Mackay–Capricorn). Intersecting the GBR10 Coral/Algae class (a class that includes algae-dominated hard bottom) with the GBR30 < 10 m surface on the 10 m grid gives 22.7 million candidate pixels GBR-wide (94.6 % of the mapped Coral/Algae class; ≈ 2,270 km^2; one benthic class within, and much smaller than, the ~10,600 km^2 of shallow hard substrate reported for the same map product by Roelfsema et al., 2021a). This figure describes the instrument's potential domain only; all claims are bounded to the ground-truthed reefs.

Two sampling facts bound every generalisation claim. Heron Reef is a high-latitude (23.4° S) lagoonal platform reef adjacent to a long-running research station, chosen for photo-record density, not representativeness; the cross-reef sets are habitat-mapping campaign reefs (a convenience sample), so cross-reef transfer is measured along one south-to-north, cross-programme axis, not over the reef population at large.

2.2 Satellite embeddings

The predictor throughout is the AlphaEarth Foundations annual embedding field (Brown et al., 2025): a 64-dimensional unit-norm vector per 10 m pixel per calendar year (2017–2025 used here). The model's inference-time inputs are Sentinel-2 optical, Landsat 8/9 optical and thermal, and Sentinel-1 C-band radar; a wider set of sources (climate reanalysis, elevation, spaceborne LiDAR, land cover, geotagged text) enters training as reconstruction targets (Brown et al., 2025, their Table S1), and the embedding does not expose which inputs carry which information. Over shallow water, C-band radar reads sea-surface roughness and thermal inputs read temperature, so non-benthic input families could in principle contribute to any signal reported here.

The Sentinel-2 ablation (§2.6) bounds what plain optics deliver and a Sentinel-1-alone baseline (§3.1) bounds the radar family from outside, but no per-sensor ablation of the embedding itself is possible without retraining the upstream model, so all skill reported here is a property of the embedding read-out, and mechanistic readings in the Discussion are flagged as interpretations.

The layers used are the public Google Earth Engine collection `GOOGLE/SATELLITE_EMBEDDING/V1/ANNUAL`, generated with model version 2.1; the published evaluation describes version 2.0, which differs in training data and targets, so all skill measured here is a property of the distributed v2.1 layers. Embeddings were retrieved from the collection's public cloud-optimised distribution (Source Cooperative) as per-reef windows spanning three UTM zones (54S–56S): survey-track extents, fixed 2.56 km attribution/auxiliary squares, and full-field Heron rasters; every exact grid, source URL, retrieval timestamp and hash is in the deposit manifest (§2.10). Windows were dequantised from the 8-bit distribution using the provider's signed-square scaling and re-normalised to unit length; masks (depth, habitat, ground-truth support) are applied at analysis time.

For state analyses, per-pixel features are the 3 × 3 neighbourhood mean of the embedding (coverage-weighted, > 40 % valid neighbours), so the 10 m tier is a 10 m grid with ≈ 30 m effective support; sensitivity is covered by the scale sweep (§2.5). All Heron analyses use this smoothed stack (the unsigned d3 screener uses raw embeddings before its own averaging); smoothed vectors are not re-normalised, so smoothed difference vectors mix angular change with neighbourhood-coherence magnitude. A raw-embedding rerun bounds the smoothing choices together, moving event-year skill by ≤ .08 and leaving the 2024 coral-loss axis unchanged (supplement). Cross-reef and cross-era windows are evaluated on raw single-pixel embeddings, so the 10 m columns of the results tables mix ≈ 30 m support (Heron) with true 10 m support (cross-reef).

2.3 Ground truth

Primary (state and change): Heron Reef photo-quadrats. Point-count benthic-cover summaries from 104,668 images across 37 named survey sites (georeferenced swim-tracks of order 250–1,000 m, not point locations), surveyed annually 2019–2025 (Golding et al., 2026; accessed via ReefCloud, an AI-assisted point-count platform (AIMS, 2024) in the lineage of González-Rivero et al., 2020); the site is the spatial cluster unit throughout. Per-image covers are normalised percentages from point-count annotation (points-per-image is fixed by the ReefCloud project configuration and not carried in the export; the PANGAEA photo-transects use 50 points per image), non-benthic points excluded. Twelve registered state channels were computed per image: hard-coral cover, *Acropora*-complex fraction, branching-guild fraction, sand, turf/epilithic algal matrix (EAM), standing-dead coral, rubble, crustose coralline algae, macroalgae, soft coral, a reef condition index (live coral / (coral + dead + rubble + macroalgae), computed where the denominator ≥ 10 %), and morphological diversity (Shannon entropy over coral morpho-taxonomic bins where coral ≥ 5 %; a morph-bin entropy, not species diversity).

Images were georeferenced onto the embedding grid; a *pixel-year* is the mean of all images falling in one 10 m cell in one survey year, retained when supported by ≥ 2 images (13,351 pixel-years; a min-1-image variant, 16,119, is the n-sensitivity check). Each ~1 m^2 image samples a small fraction of its 100 m^2 pixel, so pixel-year means are sparse samples of pixel cover, sampling noise that the measured split-half reliability (§2.8) quantifies directly.

Consecutive-year pixel pairs (3,056 transitions across six year-pairs) form the change ground truth; pairs are common-pixel intersections of successive survey coverages (pixels recur where coverage overlaps).

Surveys are austral-spring (October–November) snapshots while embeddings integrate calendar years, so an event in the first half of year *t* falls inside composite year *t* and between the year *t−1* and year *t* surveys. The event-year composite therefore averages pre-event, event and post-event months: this attenuates the measured change signal, but also means the embedding side of an event pair can carry within-composite event optics (including transient bleaching) that post-event surveys cannot see; this is the stated power limit of the bleached-cover control (§3.3).

Four off-epoch campaigns in the archive are excluded from all state and change analyses by the October–November epoch rule and named for auditability: the March–May 2024 peak-bleaching surveys (10,970 images, 22 of 37 sites) and the August 2024, March 2025 and June 2025 campaigns. The March–May 2024 surveys are the designated data for the peak-season control on the coral-loss axis, the designation specified before the control was run; sitting outside the registered epochs, that control was executed at revision as a falsification-side attack with its own confidence intervals (§2.6), not a confirmatory claim (result: §3.3).

Three definitional dependencies are stated up front: at Heron, turf/EAM is the exact sum of standing-dead (EAM on dead coral) and rubble (EAM on rubble); the *Acropora* complex is largely a subset of the branching guild; and the condition index contains hard coral in both numerator and denominator.

The *Acropora* complex is a morpho-taxonomic construct, not the genus: it sums five labels of which the largest is family-level (arborescent Acroporidae), genus-labelled morphs contribute 32 % of channel cover (label→channel mapping in the supplement), and the cross-reef target is assembled from a related but not identical morph set, so its transfer results are transfer of the complex.

These channels are correlated by construction (pixel-year Spearman: coral–branching .95, turf–standing-dead .97; full matrix in supplement); the turf/standing-dead/rubble triplet is interpreted jointly, and channel counts in the text are not counts of independent findings.

Cross-reef: PANGAEA photo-transects. Both archives are CoralNet-annotated (Beijbom et al., 2015): manually labelled training subsets, then automatic point annotation of the remaining images (50 points per image, per the source records). (i) 2017 campaigns, Cairns–Cooktown and Far Northern regions (Roelfsema et al., 2018a,b): 35,720 georeferenced images under a genus- and growth-form-resolved label scheme, aggregated to 8,965 ground-truth pixels by the same pixel rule, in 38 survey tables. The 38 units carried throughout as “reefs” are the archive’s survey tables; three reefs each contribute two tables (35 distinct named reefs), so treating tables as independent slightly overstates independence, and counts are reported as-tabled for consistency with the released ledger. (ii) 2019 campaigns, Townsville–Whitsunday and Mackay–Capricorn (Roelfsema et al., 2022a,b): 37,592 images on 29 reefs under a different label scheme and separately trained CoralNet models, 7,237 pixels. The pooled set is 67 reefs / 16,202 pixels. Because the two exports use different annotation schemes and training sets, pooled analyses use source-demeaned inference only, and no genus-level claim is evaluated against the 2019 export: its *Acropora*-complex within-source failure is itself a reported result (§3.5), the transfer claim rests on the 38 genus-resolved tables, and the pooled 67-reef row is descriptive context only.

Cross-era: Heron photo-transects 2002–2018 (Roelfsema et al., 2018c; survey design in Roelfsema et al., 2021b). The 2017 and 2018 epochs (~1,600 pixels per year) provide test data from never-trained years, a different survey method, and the earliest embedding era.

Independent checks. Reef Life Survey benthic point labels from public Squidle+ collections (RLS and IMOS, 2026; Edgar and Stuart-Smith, 2014; Edgar et al., 2020; Friedman et al., 2026; GBR 2018/2019 and Coral Sea 2019 campaigns; 3,447 points; 101 pixels meet the ≥ 4-points-per-pixel floor) provide a spot-check from a third, separately operated programme, confirmatory for sand only (§3.1). The Allen Coral Atlas benthic and geomorphic maps (Allen Coral Atlas, 2022; Lyons et al., 2020; Kennedy et al., 2021), independently produced from different sensors and methods though regionally calibrated on field campaigns related to the ground truth used here, were rasterised onto the embedding grid for map-agreement tests (§2.9).

Auxiliary data. GBR30 bathymetry (Beaman, 2017; the 2020-refresh grid under the same record) defines the < 10 m domain; grid depths reference an approximate mean-sea-level datum, not instantaneous tide; at the study reefs’ ~2–3 m tidal ranges the mask is a datum-referenced habitat definition, and the 30 m grid adds resolution smoothing. The flat/slope strata in the confound controls use the survey programme’s recorded site depths instead (ReefCloud `depth_m`; reef flat < 3.5 m).

NOAA Coral Reef Watch Degree Heating Weeks (NOAA Coral Reef Watch, 2018; Liu et al., 2014; Skirving et al., 2020) identify event years, auditable at the site: maximum annual DHW at Heron (single covering 5 km cell) is 7.6 in 2020 and 11.4 in 2024 against ≤ 0.8 in every other study year, including 0.5 in 2022, when the GBR-wide event spared the Capricorn–Bunker sector (the same extract shows the stress elsewhere; table S12); the §3.5 attribution dose is a separate per-window February–May maximum. The event/quiet split follows the conventional DHW ≥ 4 alert threshold (2020 = Alert Level 1, 2024 = Alert Level 2) with no discretionary cases.

Annual Sentinel-2 L2A composites (four 10 m bands) provide the optical-baseline ablation; cyclone exposure and crown-of-thorns pressure (§3.5) use the Bureau of Meteorology tropical-cyclone database (Bureau of Meteorology, n.d.; Courtney et al., 2021) and AIMS long-term manta-tow data (AIMS, 2017). Every dataset, role and access route is in the data-availability statement; per-run dataset consumption is recorded in the released ledger (§2.10).

2.4 Decoding models

Simple decoders were used throughout. Continuous channels use ridge regression on the standardised 64-dimensional features ($\alpha = 10$; a four-order-of-magnitude α sweep moves held-out skill by ≤ 0.011). Class outputs use one-vs-rest ridge scoring evaluated by AUC. No deep models, feature engineering or hyperparameter search: the survey measures what the embedding carries, not what an optimised estimator can extract.

Two skill metrics are reported: Spearman rank correlation on held-out data (rho), and a *detection score*, the sensitivity at a fixed 10 % false-positive rate for the ecologically relevant quartile (lowest-quartile cover for hard coral and the condition index; highest otherwise). Because the quartile and alarm threshold are computed on the held-out set (threshold at the 90th percentile of held-out negatives), this is a discrimination summary (a fixed ROC point), not an operational detection rate; a training-fixed-threshold variant was measured for both regimes (state thresholds transfer, change thresholds do not; §3.3).

2.5 Spatial scales

Every test was run at six scales: 10, 20, 30, 50, 70 and 100 m. Blocks of $k \times k$ pixels were formed on the embedding grid, anchored to the window origin (fixed tiling); block ground truth is the mean of member pixel-years and the block feature the mean embedding, requiring ≥ 2 ground-truthed pixels per block (support sensitivity in §3.4). Each channel is reported at every scale rather than at its best scale.

2.6 Fixed validation protocol

Every candidate passed the same battery. *Spatial holdout:* plain leave-one-site-out cross-validation (LOSO; 37 named, spatially separated sites) is the headline holdout: every headline skill comes from a model that never saw the test site. This controls site identity, not spatial proximity (site pixels can lie within tens of metres of a neighbour's, and the 3×3 halo can straddle a boundary), so spatial isolation is measured by a 600 m buffered LOSO variant (all training pixels within 600 m of the held-out site removed), whose numbers are reported alongside the headline values (§3.1); channels whose apparent skill is spatial leakage die under it (macroalgae and soft coral do, at Heron).

Spatio-temporal holdout: site + year double holdout (train on other sites in other years only; unbuffered).

Confound controls: depth-stratified re-tests (flat vs slope at 3.5 m recorded depth); a site-identity floor (a predictor given only each site's mean, isolating within-site signal from between-site ranking); label permutation; and a Sentinel-2 ablation against three baselines (four-band annual median composite; a strengthened multi-temporal percentile stack of the same bands; and a revision-round widened variant appending the same percentile features of the six 20 m red-edge, narrow-NIR and SWIR bands, 30 features; L2A/Sen2Cor is a land atmospheric correction, so increments are relative to strong practical optical baselines, not the strongest conceivable one).

Robustness: regularisation sweep; minimum-image sensitivity; site jackknife; ±1-pixel georeferencing jitter (moves 10 m skill by ≤ .007); a nonlinear-decoder check (gradient boosting vs ridge under identical buffered folds); a buffer ladder (600/900/1200/1800 m); and a persistence control (previous-year, next-year and time-averaged embeddings).

Generalisation: leave-one-reef-out replication across 38 (genus-resolved 2017 GT) and 67 (pooled, source-demeaned) reefs; a reef-identity floor; prevalence screening (mean cover ≥ 5 % and non-zero in ≥ 40 % of pixels); cross-era transfer (2019–25-trained decoders on 2017/18 ground truth). Change-specific attacks are in §2.7.

A channel is reported at a tier only if it passes the gates under the full battery; conditional channels are labelled with their condition, and a condition derived post hoc from the same data is either demoted to the supplement (rubble prevalence, §S12) or labelled post hoc with confirmation pre-registered (macroalgae abundance, §3.5).

Several elements were added during revision as falsification-side attacks on the registered claims, among them the buffer ladder, persistence control, threshold-transfer and cross-reef deployment tests, maximum-power quiet attack, bleached-cover controls, sign-test hardening of the reef-identity floors, and the Sentinel-1-alone and widened Sentinel-2 baselines. Attacks that produced new descriptive numbers are reported outside the confirmatory family with their own confidence intervals, flagged as post hoc wherever they appear; none raises any registered claim above the level its registered test earned. A complete list of every revision-round test is released with the supplement (§S6) so the two analysis generations are separable.

2.7 Change analysis

Change decoding operates on the embedding difference vector Δe = e(year b) − e(year a) for consecutive-year pixel pairs, demeaned within each transition (removing the year-pair mean shift, which carries tide, water and sensor conditions). The demeaning is transductive (the mean includes test pixels) and its support is the ground-truthed pixel set, not the full window, so what the decoder estimates is change relative to the average shift across the surveyed pixels; a deployment analogue (demean over the full field) is untested, and deployed change maps should be read as contrasts within the mapped extent.

Signed per-guild change decoders (Δ hard coral, Δ *Acropora*, Δ branching, Δ condition, Δ turf, Δ standing-dead, Δ sand) were fit by ridge on Δe and evaluated by leave-one-transition-out cross-validation. The record contains exactly two event transitions, so every event-transition number is a one-event-to-one-event transfer: conservative rather than leaky, and generalisation from a single training event.

Two summary axes were fit the same way: a *coral-loss axis* (trained on event-transition coral loss; functionally a substrate-conversion detector, since the target is live-cover loss, which includes removal as well as mortality, and live cover includes bleached-but-living colonies) evaluated as a loss detector, and a *recovery axis* (trained on one rebound transition, tested on the other) evaluated as a gain detector. The unsigned screener d3 is the cosine distance between raw annual embeddings, 3 × 3 averaged.

Event gating was tested, not assumed: every change output was evaluated separately on the two thermal-stress event transitions (2019→20, 2023→24, identified by DHW) and the four quiet transitions (specificity nulls); an adversarial sign-coherence test probed apparent quiet-year skill at coarse scales; and a maximum-power quiet attack bounds any residual quiet-year signal from above (design and decomposition with the result, §3.5). Site-demeaned re-tests separate within-site change texture from between-site ranking.

Because the ground-truth scheme labels bleached colonies separately, a bleached-cover channel was differenced alongside coral as a control on the coral-loss axis (cover loss or whitening?; power limit stated with the result, §3.3). Both gate-opening events are thermal; behaviour under other acute disturbances (cyclones, predation) is untested, and all change products are scoped to thermal-stress event years.

2.8 Statistical inference

No naive p-values are reported anywhere. All inference is by cluster bootstrap: B = 2000 resamples over the clustering unit that carries the dependence (sites at Heron, 37; reefs in cross-reef tests, 38 or 67; spatial blocks of 200–300 m where no site structure exists), with 95 % percentile confidence intervals and a one-sided cluster p of (k+1)/(B'+1), where B' is the number of valid resamples (degenerate draws discarded; B' = B in almost all cells), so the smallest reportable p is ≥ 0.0005.

Cluster counts are stated with the results in the text and summarised in the supplement (§S2); sub-analyses on fewer than ~15 clusters (the 9-reef rubble-prevalence stratum, the 13-deployment point-label spot-check) are flagged as approximate (percentile intervals under-cover at small cluster counts). AUCs use the same procedure around a Mann–Whitney estimate.

Ground-truth reliability was measured directly by split-half correlation with Spearman–Brown correction, and headline skills are additionally reported disattenuated for it (corrected for that measured ground-truth noise). Holm correction was applied post hoc within each channel × test family across the scale ladder and is reported strictly as a family-size disclosure (the bootstrap p-floor times family size caps adjusted values at ≈ 0.0025–0.003, so claims at the floor cannot fail by construction; full table in the supplement).

2.9 External map agreement

Allen Coral Atlas benthic and geomorphic polygons were rasterised onto the embedding grid (~322,000 window pixels at Heron). Agreement was tested in both directions, decoder-side (do this study's decoders separate Atlas classes?) and embedding-side (are Atlas classes directly decodable under 200 m spatial-block cross-validation?), both scored by cluster-robust AUC. One lineage fact is disclosed: the embedding model's training-site sampling drew on Atlas-derived reef extent (Brown et al., 2025); the Atlas informed *where* the model sampled, not what it was trained to predict, so Atlas agreement is between independently produced products with shared sampling ancestry, not fully independent validation.

2.10 Software and reproducibility

All analyses run from one shared Python library (ridge fitting, block aggregation, cluster bootstrap, dataset loaders) so every run shares identical joins and preprocessing; the released reproduction pack includes a self-contained companion library implementing the same conventions. Every analysis script carries its registration in its header, writes a per-run log, and appends structured result rows (output, test, scale, metric, value, CI, p, n, datasets consumed) to a machine-readable ledger from which the results tables are assembled mechanically. The reproduction scripts and ledger are released at https://doi.org/10.5281/zenodo.22065301; the pack reproduces the fully public tier end-to-end and executes the public-test-data results from released decoder weights; the Heron-restricted tables require the custodian data. Because the Earth Engine collection can be revised by the provider (the v2.0→v2.1 change has already occurred), the exact embedding windows used are archived at https://doi.org/10.5281/zenodo.22065348 under the dataset's CC-BY 4.0 licence, with a manifest of per-window source URLs, retrieval timestamps, georeferencing and SHA-256 hashes, so every result remains reproducible against its exact inputs. Trained decoder coefficients and calibrated thresholds are released as derived parameters, valid for the archived v2.1 windows they were trained on; predictions on freshly downloaded layers are unvalidated until re-checked against the deposit. Analysis code was implemented and run with the assistance of AI coding tools (Cursor, with the Fable 5 and Grok 4.6 models); all analyses were designed, registered, reviewed and interpreted by the author, who takes full responsibility for them.

2.11 Post-registration validation campaign

After the registered analysis and its revision rounds were closed, a further campaign of 36 runs tested the catalogue's external transfer and temporal limits against datasets the registered study never touched: the AIMS Long-Term Monitoring Program manta-tow series (raw extract, 528 reef-years at 184 reefs, 2017–2023, plus the AIMS dashboard modelled series through 2025), the AIMS LTMP fixed-site photo-transect archive (306 sites at 102 reefs, 2017–2023), Allen Coral Atlas class packs at seven never-trained reefs, NOAA Coral Reef Watch DHW rasters, eReefs water-quality climatology, and the GBR10/GBR30 products as domain rasters. Each run pre-stated its design and pass gates in its script header before results existed; inference follows §2.8 with reefs (or sites) as clusters. External site read-outs average decoded cover over square patches (50–510 m) on the smoothed 10 m grid, centred on the published site coordinates, not over survey-transect footprints. Campaign results carry their own confidence intervals, are never promoted into the registered confirmatory family, and are Holm-corrected within each campaign round (r81): every campaign number quoted here survives the correction; failing rows are labelled leads, and the full sweep is released with the supplement (`tableS16_holm_campaign.csv`). Summary in §3.7; run-by-run detail in supplement §S13; rows in the released ledger.

---

3. Results

Reporting conventions: correlations are Spearman rho on held-out predictions; p-values are cluster-bootstrap (§2.8; the floor p = 0.0005 means no resample crossed the null); "LOSO" is plain leave-one-site-out, "DH" the site + year double holdout; detection is sensitivity at a fixed 10 % false-positive rate (§2.4).

3.1 Benthic state channels

Of twelve registered benthic state channels, eight are catalogued at one or more scales under the full validation protocol, and six of these validated beyond the training reef (counts include definitionally linked channels, §2.3; held-out *predictions* for the coral-guild block correlate at .97–.99, so the catalogue spans fewer effective axes than channels; supplement §S3; a post-registration partialling analysis shows they are nonetheless not one axis, §3.7). Two further registered channels, crustose coralline algae and morph-bin entropy, pass gates at the training reef but with the weakest effect sizes and no pixel-level transfer; they are reported in the supplement only (tables S1–S2). Skill at the core site (Heron Reef; 13,351 pixel-years, 37 site clusters, 7 years) rises steadily with block size for every channel (Fig. 1):

Channel	10 m (LOSO/DH)	50 m	100 m	Cross-reef, 38 reefs (10→100 m)	Cross-era 2017 (10/50 m)
Hard coral	.73/.57	.80/.62	.84/.64	.55→.60	.76/.84
Acropora complex	.74/.66	.81/.71	.84/.74	.45→.46	.69/.78
Branching guild	.70/.58	.78/.63	.82/.66	.51→.52	.68/.77
Sand	.69/.66	.73/.70	.74/.71	.61→.69	.71/.75
Turf/EAM	.63/.49	.72/.56	.75/.58	(no comparable class)	—
Standing-dead coral	.61/.47	.69/.55	.73/.57	.33→.41	.53/.64
Condition index (live-coral ratio; §2.3)	.63/.43	.70/.46	.73/.47	.51→.54	.68/.79
Rubble	.48/.42	.54/.48	.57/.51	no unconditional transfer (post-hoc lead: §S12)	.23/.30

The 20, 30 and 70 m tiers lie on the same monotonic curves (supplement). Every cell shown has a cluster CI excluding zero (cluster $p \leq .002$, most at the .0005 floor). Holm-adjusted p-values are tabulated in the supplement as a family-size disclosure (§2.8); detection scores and revision-round tests sit outside that family and carry their own confidence intervals (§S6).

Under the 600 m buffered LOSO variant the core channels retain their skill (coral .66/.72, *Acropora* .69/.74, sand .68/.72, turf .57/.65 at 10 m / 50 m), while macroalgae (.01–.02) and soft coral collapse and are treated as leakage-confirmed at the training reef (macroalgae re-enters conditionally; §3.5). Detection scores at 10 % FPR rise with scale: sand 87→96 %, *Acropora* 59→81 %, branching 55→74 %, hard coral 51→72 % (10 m → 100 m).

Two constructs require comment. Standing-dead coral and rubble are both EAM-covered surfaces, yet only standing-dead transfers cross-reef unconditionally; the ground truth separates the two and neither is a live-coral inverse (pixel-year correlations .27, −.28, −.31), and the candidate physical carrier is discussed in §4.1.

A genus-strict *Acropora* target decodes at .56/.71 (10/50 m) versus .74/.81 for the complex, confirming the channel must be reported as a morpho-guild complex, not genus *Acropora* (§2.3; construct detail in supplement table S9).

A habitat-composition control addresses whether the flagship skill is merely between-habitat contrast: restricted to pixels the Allen Coral Atlas classifies as Coral/Algae (40 % of pixel-years, target spread preserved), the hard-coral decoder holds at .71/.82 (10/50 m) against .73/.80 in the full domain, and the condition index is if anything stronger within-class: within-habitat gradation, not habitat-class separation. Sand shows the mirror image, collapsing within the class as its variance there vanishes.

Generalisation. The channels were stress-tested along four axes (independent to different degrees; the third is a sand-only confirmation). (i) *Space:* leave-one-reef-out replication at 67 reefs across three regional groups (source-demeaned pooled rho .34–.54 for the core channels; the *Acropora*-complex transfer claim rests on the 38 genus-resolved survey tables, §2.3). Pooled numbers include between-reef ranking; the pixel-level quantity to quote is the *reef-identity floor* (Fig. 2d): median within-reef rho on never-trained reefs of .30 for hard coral, .47 for sand, .31 for standing-dead, .31 for the condition index, .19 for branching and .16 for the *Acropora* complex. This is roughly half the within-programme skill for the strong channels, and the number any no-local-ground-truth deployment claim must be read against (§4.2).

A revision-round hardening (supplement §S6) attaches reef-resampled intervals and one-sided sign tests against a coin-flip null: hard coral median .30 (95 % CI .18–.41; 35 of 38 reefs positive, $p = 3 \times 10^{-8}$), sand 37/38, standing-dead, branching and condition 31–33/38; the *Acropora*-complex floor is the weakest (26/38, $p = .017$, below the study's $p < .01$ convention) and is read accordingly.

(ii) *Time and survey programme:* decoders trained on 2019–2025 photo-quadrats predict 2017/2018 photo-transects (never-trained years, a different survey method, the earliest embedding years) at rho .53–.84 for coral guilds, condition, standing-dead and sand. (iii) *Independent annotation programme:* a point-label spot-check from a third programme, run entirely on public PANGAEA-trained decoders (a fully public replication path), confirms sand (+.48, CI +.05 to +.70; 13 clusters, approximate); coral is in the expected direction but has too little data to confirm (n = 101 pixels).

(iii) *Independent map product:* the sand decoder agrees with the Allen Coral Atlas benthic map at AUC .962 over 322,000 pixels, and the embedding reproduces every mappable Atlas class directly at AUC .87–.97 (200 m spatial-block cross-validation; §3.2; shared-ancestry disclosure, §2.9). A feature-ablation control bounds what this certifies: plain Sentinel-2 nearly ties on sand (AUC .958) and beats the embedding on the optically derived Coral/Algae class (.94 vs .66), so Atlas agreement is a consistency check for optically recoverable channels, and the burden of validating embedding-specific skill rests on the in-water ground truth.

Composition of the skill ceiling. Split-half reliability of the photo-quadrat ground truth is .78–.93 (Spearman–Brown, full image count) for most channels. Correcting held-out correlations for this measured unreliability moves hard coral from .73 to .78 and *Acropora* from .74 to .80: even against noise-free ground truth, decodability would top out near .8 at 10 m.

The correction is approximate (a classical independent-error model, blind to shared errors such as georeferencing offsets, dividing a Spearman skill by a Pearson-based reliability; construction in the supplement), so the ceiling reads ≈ .8, not an exact bound. To that accuracy, the remaining gap is genuine signal limitation, not ground-truth sampling noise (exception: soft coral, whose ground truth is itself unreliable, split-half .42).

Ablation. Replacing the embedding with Sentinel-2 baselines under identical folds costs skill on every channel except sand. Against a plain four-band annual median composite the embedding adds +.14 to +.27 rho across the catalogue; against the strengthened multi-temporal baseline (per-scene-normalised 10th/50th/90th percentiles of the four 10 m bands) it still adds +.07 (rubble) to +.16 (condition index), with +.11 to +.14 on the coral guilds (per-channel increments in the supplement).

Widening that baseline with the six 20 m red-edge and SWIR bands (same construction, 30 features; supplement §S6) gains the optics only +.02–.04, an expected ceiling over water: even shallow water absorbs SWIR almost completely, so the red-edge bands carry most of the effective widening. The increment holds at +.08 to +.11 (paired cluster CIs excluding zero) on every catalogue channel except rubble and sand: rubble's +.04 spans zero and is excluded from the claim against the widened baseline. Sand runs the other way (embedding .69 vs S2 .73–.77), a brightness signal readable without the embedding; sand is retained as a product channel but is not evidence for the embedding method.

Whether the increment over optics rides on the embedding's radar inputs (§2.2) was bounded at revision (supplement §S6): a Sentinel-1-alone baseline (per-scene VV/VH/ratio annual percentiles) decodes the catalogue channels only weakly (rho .08–.26, consistent with sea-state and exposure zonation), and adding radar to the strong optical baseline moves every catalogue channel by under +.03 rho (the supplement-only crustose-coralline channel gains +.12; §S6); the increment over optics is not radar-carried.

Model capacity. A gradient-boosted decoder under identical 600 m buffered folds gains +.04–.05 rho over ridge on the coral guilds and ≤ .015 on sand and turf. The coral-guild gain exceeds the pre-stated ±.03 margin, so a small nonlinear component is reported as real, bounded, and exploitable in deployment; it does not alter the ceiling analysis, which the disattenuation bounds independently.

Persistence structure. A feature-swap control bounds what the cross-sectional skill means (Fig. 2c): fed the previous year's, the next year's, or the 2019–2025 mean embedding instead of the matching year's, the coral decoder still reaches rho .74–.75 against .76 same-year on the common subset, and sand is indistinguishable across all four. Cross-sectional state skill is therefore dominated by persistent between-pixel habitat structure rather than year-specific state: the state product is an annually refreshed habitat-structure map, and the year-specific information of the annual layer is concentrated in the event-gated change regime (§3.3, §3.5).

3.2 Auxiliary layers: depth and geomorphic zone

Two non-ecological layers decode near the ceiling and serve as scaffolding: water depth / reef-zone class (slope-vs-flat AUC .967 at 10 m, rho +.80), and the nine-class geomorphic zonation (one-vs-rest AUC .87–.99 per zone under 200 m spatial-block cross-validation, macro-AUC .945, measured as agreement with the Atlas geomorphic layer; §2.9 disclosure applies). One provenance caveat: the embedding's inputs include radar and its training targets an elevation source (§2.2), so depth decodability may partly read bathymetric surface signatures rather than water-column optics; immaterial to the layers' role as scaffolding, but not evidence of optical bathymetry retrieval. Their strength motivates the depth-stratum control applied to every ecological channel: all catalogue channels retain within-stratum skill, so no ecological channel is reducible to a depth map (exception: supplement-only morph-bin entropy, slopes only).

3.3 Change channels

Year-over-year change decoding operates under a strict regime split. In the two documented bleaching-event transitions (2019→20, 2023→24), the signed change in hard coral, branching guild and condition index is recoverable from the embedding difference vector (leave-one-transition-out; both events cluster $p < 0.01$ at multiple scales); turf and standing-dead change join at 20–30 m only. With two events in the record, each event row is a one-event-to-one-event transfer (§2.7). Because of the definitional links of §2.3, the five passing channels reduce to two effectively independent findings, a coral-loss axis and a substrate-conversion axis (§4.1).

In the four non-event transitions the same decoders flag nothing at or below the false-positive budget, but the specificity structure is informative (Fig. 3a): the two rebound transitions (2020→21, 2024→25) score *below* chance on the loss task (AUC .29–.35; cluster CIs exclude 0.5 at 10, 20 and 50 m; the axis reads first-year regrowth as anti-loss; §3.5, §3.6), while the two true-quiet transitions sit at or just below chance (AUC .38–.49; CIs span 0.5 except at 30 m). Pooled "quiet" AUCs below 0.5 reflect this rebound component, not false alarms (detection stays at 3–13 % against a 10 % budget).

Signed change	10 m	20 m	30 m	50 m	100 m
Hard coral	.36/.39	.48/.60	.55/.49	.51/.57	.60/.52
Branching	.25/.28	.35†/.52	.40/.45	.31/.36	.38/.44
Condition index	.37/.19†	.51/.48	.55/.45	.52/.45	.64/.38
Turf/EAM	✗	.48/.33	.50/.34	✗	leaks
Standing-dead	✗	.51/.34	.53/.36	✗	leaks

† shown for completeness; raw cluster $p \geq .01$ (branching 2019→20 at 20 m, $p = .027$; condition 2023→24 at 10 m, $p = .016$). The 70 m tier is in the supplement (event gate passes for 2023→24; 2019→20 under-supported at that block size).

Two scale bounds define the operating band. At 10 m, site-demeaning collapses signed skill to .04–.09, so the 10 m signed map ranks sites, not pixels; genuine within-site signal appears only at the block tier (demeaned .13–.25 at 50 m). At 100 m the event gate itself leaks: quiet-year confidence intervals exclude zero for three guilds. Change products are therefore valid at 20–50 m only, in thermal-stress event years (scope: §2.7).

Within that band, the coral-loss axis discriminates ≥ 10-point loss blocks in the 2024 event at 20 m at AUC .83 (cluster CI .69–.92); its detection sensitivity at the 10 % false-positive budget is estimable only to a wide site-clustered interval (13–85 %; few site clusters carry the losses), against 3–13 % in non-event transitions. The two events are not symmetric: 2019→20 passes the registered event gate at 10 m and 50 m (AUC .65/.73, cluster $p < .01$) and is under-powered at 20 m (AUC .66, $p = .07$).

Nor do alarm thresholds transfer between events: because per-transition score scales shift, a threshold fixed on one event either collapses sensitivity (16 % on 2024) or blows the false-positive budget (39 % realised FPR on 2020) on the other (Fig. 3b). The change product is therefore a *ranked triage map* (top-quantile flagging within the new layer; Fig. 4), not a fixed-threshold alarm. Ground-truth reliability and the optical ablation that the skill-ceiling and increment arguments rest on are shown in Figs. 5 and 6.

State channels do not share this problem: a hard-coral alarm threshold fixed from training folds transfers cleanly within the training programme (58 % detection at a realised 10.7 % FPR); deployed beyond the programme and region, its false-positive rate drifted to 13–15 % on the 38 never-trained reefs with detection not distinguishable from chance (drift and a per-reef recalibration variant that restores the false-positive budget, not detection: table S5, §S6).

Two bleached-cover controls bound what the axis reads: controlling the axis score for surveyed bleached fraction leaves the loss association unchanged both at survey time (2023→24 partial rho −.60 versus −.60 raw) and in the designated peak-season control on the March–May 2024 surveys, where whitening is present (20 m partial −.36, cluster CI −.58 to −.13, versus −.38 unconditioned; reverse partial spanning zero). The axis reads realised cover loss rather than whitening, and blocks that bleached without losing cover show no elevated loss score (full cells and power limits: table S14, §S6).

The task definition is not load-bearing: sweeping the loss threshold and the false-positive budget degrades the 2024 result gracefully (AUC .80–.85), with no knife-edge at the registered −10-point/10 % choice. The 20 m detection gain over 10 m is attributable to two-sided noise averaging, not ecological grain: the ground-truth change field has no within-site spatial autocorrelation in either event.

Change in sand is undetectable everywhere (event CIs rule out rho > .24 in 2019→20 and > .13 in 2023→24 at 10 m), and the unsigned change screener generalises to only one of the two event types; both are negative results with measured upper limits.

3.4 The scale architecture

Skill increases monotonically with block size, so the product architecture is a design choice rather than an optimum: a 10 m drill-down tier (a 10 m grid with ≈ 30 m effective support; local contrasts reflect year-tracking more than neighbour-to-neighbour texture), a 50 m primary tier (LOSO .54–.81 across catalogued channels), and 100 m regional roll-ups. The site-identity floor makes the meso-scale caveat quantitative: for the coral guilds, nearly all pixel-level skill is between-site ranking plus year tracking (site-floor increment +.01–.02 rho at 10 m), whereas turf and standing-dead carry a genuine within-site increment (+.17–.21), read as within-site year-tracking more than static texture. Cross-reef transfer gains with scale are real but smaller than at the training reef. Measured ground-truth reliability (§3.1) explains part, but not all, of the block-scale gains; the remainder is embedding-side noise averaging. Coarse-tier support is sparse (blocks require only ≥ 2 ground-truthed pixels; restricting 50 m blocks to full support costs .04–.07 rho), so coarse-tier skills are skills at predicting sparse-pixel aggregates, not exhaustive block means.

3.5 Conditional channels and validity limits

One channel carries an explicit validity condition established by falsification, and one transfer lead is held in the supplement. Rubble fails naive cross-reef transfer (+.05); a post-hoc re-test conditioned on rubble prevalence recovers a positive transfer signal but rests on 9 prevalent-reef clusters, below this study's own cluster-reliability line, so it is reported in the supplement only (§S12) as a lead, with out-of-sample confirmation pre-registered; away from the training reef, no rubble product is offered.

Macroalgae is killed by a 600 m spatial buffer at the training reef, where it is rare, but transfers on the 29 reefs where it is abundant (leave-one-reef-out +.41, p at the bootstrap floor; median within-reef rho +.31 with 28 of 29 reefs positive, sign-test $p = 6 \times 10^{-8}$): an abundance-conditional channel, not a full-cube pass (the training-reef buffer kill stands). The abundance rule was derived from these data and is labelled post hoc, with confirmation pre-registered; one confound is stated plainly: all 29 reefs come from a single southern-GBR campaign (one region, year and annotation programme), so generalisation awaits a second campaign.

Four negative results bound the instrument. (i) Quiet-year change is undetectable at every scale, in all four non-event transitions of the 2019–2025 record, and, by the post-registration lag sweep, at every quiet temporal separation in the record (lags of one to three years; every longer lag spans an event), with trend estimators faring no better (§3.7). This is an embedding-side limit, not a ground-truth power limit: quiet-year ground-truth deltas are themselves measurable (split-half reliability .35–.55), yet decoders trained on them find nothing. At most, any undetected quiet-year signal is small: pooled across the four quiet transitions, the upper 95 % confidence limit falls below rho = .16 at 10 m for every guild (most below .09), and below .26 at 20–50 m (estimation-CI upper edges, not a formal equivalence test). A maximum-power attack (decoders trained *only* within quiet transitions, plus a nonlinear variant under the same folds) still finds nothing under the registered linear protocol (pooled rho .01–.02, every CI spanning zero), so the quiet-year null is stated as a property of the registered linear read-out. The nonlinear variant recovers at most a small residual inside the bounds above; it emerged from a revision-round search, would survive a Holm correction over that grid, and is withheld under the post-hoc rule with its confirmatory test pre-registered and the grid tabulated (§2.6, supplement §S5).

(ii) Recovery (coral gain) detection did not validate: continuous rate prediction fails (rho .05–.16, n.s.) and rebound-era detector transfer is unreliable (supplement); the post-registration campaign closed the direction externally, with true gains ranking below chance and a directional look-alike bias measured at the training reef (§3.7).

(iii) Genus-level channels could not be trained or evaluated on the 2019 export: the *Acropora* complex collapses to +.01 within that source while transferring at +.19 from the genus-resolved 2017 tables, and injection experiments show random label noise cannot produce this failure, so the annotation errors of this export are systematic (scoped to this export and construct; both archives are CoralNet-annotated, §2.3, so the failure attaches to this export's label scheme and training, not to machine annotation as such); total-cover and substrate channels are robust to the same labels.

(iv) Reef-scale attribution from window-mean change is not supported at the grain tested: across 7,611 window-transition pairs (~960 2.56 km reef windows × consecutive-year transitions, 2017–2025; dose definition in §2.3), thermal-stress dose, crown-of-thorns pressure and cyclone exposure show no within-site association with window-mean embedding change robust to the choice of demeaning (the crown-of-thorns join is far smaller than the other two screens, so that null is weaker evidence). The null is at whole-window aggregation, far coarser than the 10–50 m tiers where the decoded signals live; it bounds window-mean screening rather than pixel-scale pressure signatures. A post-registration re-test with per-pixel loss-axis footprints partially revises the thermal side: they track the spatial DHW gradient in moderate years and saturate in the severe event (§3.7).

Finally, two methodological results with general relevance. A naive random-pixel train/test split inflates apparent skill by +.10–.28 rho and up to doubles detection rates relative to spatially separated cross-validation (Fig. 2a), a direct quantification of spatial leakage, replicated beyond the training reef (pooled rho inflated by +.07 to +.23 on the 38-table campaign set, every channel; supplement §S6).

The buffer radius was laddered (600/900/1200/1800 m; Fig. 2b): skill is stable through 900 m (coral .66 → .63), and the collapse at the widest rungs tracks the buffer carving away most survey-track training data rather than leakage (sand is immune; rung-by-rung numbers in the supplement); the disambiguating evidence is cross-reef transfer (§3.1), which retains pooled rho .34–.54 with zero same-reef pixels, bounding any leakage contribution to cross-site claims.

Pooling ground-truth sources with different annotation schemes inflates substrate-channel skill to .75–.82 through pure source contrast; all pooled results use source-demeaned inference, and per-source decoders outperform pooled training wherever the ground truth is clean.

3.6 Demonstration: separating coral-gaining from coral-losing reef in event years

Within event transitions, combining the coral-loss axis with a rebound-trained recovery axis separates pixels that gained coral from pixels that lost coral at AUC .672/.729 (2019→20 / 2023→24, both cluster $p \leq .006$ at 10 m; stronger but thinner at 50 m; Fig. 3c), with rebound-year controls at chance. This is a bounded demonstration rather than a product: the embedding difference vector carries directional ecological information beyond change magnitude.

3.7 External validation and temporal limits (post-registration campaign)

A campaign of 36 runs after the registered analysis closed (§2.11; run-by-run detail in supplement §S13) tested the catalogue against external monitoring archives it had never touched. All numbers below carry their own confidence intervals and sit outside the confirmatory family; a closing multiplicity sweep (r81) applied Holm correction within each campaign round, every number quoted here survives it, and the sweep table is released with the supplement.

External state levels transfer; calibration does not. Read at 289 never-trained LTMP fixed photo-transect sites (1,047 site-years, 102 reef clusters; coordinate-precision screen in §S13), the Heron-trained coral decoder recovers site-level cover at rho +.25–.26 across 50–510 m patches (§2.11), and at +.376 [+.205, +.513] at sites within mapped reef-slope geomorphology; manta-tow reef windows carry the same signal at +.17–.20. The attenuation is genuine transfer loss: a protocol-matched benchmark at Heron (same patch construction, its own years and folds) scores +.869. Both grains should be read against the measured inter-programme agreement: the two AIMS survey instruments agree with each other at only +.712 on levels, so site-level skill is roughly a third of that agreement, and manta-window skill roughly a quarter. An elimination battery removes coordinate jitter, patch size, water depth (skill holds to ~9 m), survey timing, a water-clarity climatology and training breadth as explanations, leaving habitat and grain mismatch as the residual candidates (§S13). Transfer has measured reach: leave-region-out passes in both directions, and skill persists with every training reef at least 200 km away (+.373 [+.235, +.485]). Absolute units do not travel: the internal maps are nearly unbiased (pixel grain: slope 0.94, MAE 10.4 points, 90 % intervals covering 90.7 %; site grain: slope 1.00, MAE 6.4), but externally the slope falls to 0.29 with a +14.5-point over-prediction, so off the training programme the state product ranks sites rather than measuring them. The ranking still adds information: at the 930 of those site-years with a mapped GBR10 class in the surrounding patch, the annual index predicts measured coral cover at rho +.320 [+.185, +.433] where the static habitat-class fraction carries none (−.020; paired difference +.340), though the two products differ in kind.

Year-over-year trajectories fail externally, with a measured directional bias. Transition-demeaned deltas and multi-year trends track the surveys at neither external grain (manta deltas −.10 with CI below zero, per-reef trends −.43 [−.59, −.23]; fixed-site deltas spanning zero), and reefs or sites that truly gained ≥ 10 points of coral rank *below* chance (gain AUC .42–.44; fixed-site .43 [.37, .49]). The failure belongs to the read-out, not the reference: the two survey instruments agree with each other on the same deltas (+.538) and trends (+.657). A pre-stated test at Heron identified a look-alike residual consistent with the bias: given true cover, the coral decoder over-predicts where turf-covered standing-dead skeleton is present (partial rho +.398 [+.172, +.575] over all 2025 pixels; the companion rebound-change gate failed, and the like-for-like external test was directional but marginal, so the mechanism is measured at the training reef and inferred elsewhere, §S13), and Heron's own post-event maps rebound toward baseline faster than the ground truth. No combination of catalogue channels rescues the gain direction; one succession-corrected composite (coral − turf) does make external site-level *loss* detection significant (AUC .635 [.549, .710]), a bounded loss-side lead. Trajectory read-outs from decoded state indices are therefore directionally biased rather than merely noisy, and apparent gains should be distrusted wherever local change ground truth is absent.

Reef-scale change detection is bounded, at the calibration reef only. Aggregation recovers what pixel statistics cannot: at Heron, site-mean indices track the two lag-1 event transitions pooled at rho +.868 [+.76, +.92] (53 site-windows; regression attenuation slope .63 against a site-scale quiet SD of 4.5 index points), and the median of the full-reef 2023→24 difference map is −14.9 points against a reef-mean quiet-transition SD of 2.8 (event tracking ratio .80). The implied minimum detectable change (1.96 × quiet SD / attenuation, the conventional two-sided α = .05 threshold, estimated from seven quiet windows) is about 14 true points at site scale and about 7 at whole-reef scale, at any speed the record can test: the quiet floor is flat across the measured lags of one to three years, so a slow decline surfaces once it accrues past the floor even though no yearly map pair shows it. The scope is strict: the same estimator, run without ground truth at 508 external reef windows, shows quiet-year reef-mean swings near 15 points (robust to domain masking, unexplained by a water-clarity climatology, and too large for within-window error; §S13), consistent by elimination with a per-year whole-window offset. The reef-scale detection bound therefore does not generalise without local calibration, and external windows show no 2023→24 event contrast in the index.

Event-regime scope. The coral-loss axis outperforms plain state differencing at the severe event (paired AUC difference +.068 [+.022, +.132], p = .0025), and temporal generalisation is clean: decoders trained only on past years read a never-trained year at undiminished skill, including across the unseen 2024 event, with macroalgae the named exception

(§S13). The axis footprint tracks the spatial thermal-stress gradient in moderate DHW years (rho +.19–.28 across ~500 reefs; year-by-year cells and one disclosed low-variance anomaly in §S13) but saturates in the severe 2023→24 event, with a median flagged fraction of .87 per reef window and nothing left to rank; windows extending more than about a year past an event decay toward baseline as the annual composite mixes in the recolonised surface, so detection has a roughly one-year shelf life. Cyclone-driven structural loss remains untested: at the grain testable, the forcing does not resolve into measured coral change in any instrument. Two further results bear on the catalogue: decoded sand agreement with the Allen Coral Atlas extends to all seven tested never-trained reefs across ~10° of latitude (AUC .64–.85, every CI > 0.5; one window re-cut, disclosed), and a partialling analysis shows the channels are not one latent axis: every non-derived channel keeps skill after the coral prediction is removed (partials +.19 to +.80; §S13), with branching the exception, re-scoped as a coral-nested correlate.

---

4. Discussion

4.1 A two-regime instrument

The central empirical result is a regime structure, not a single skill number. In the *state regime*, a general-purpose annual embedding carries enough information about the shallow benthos to support guild-level cover mapping: linear read-outs recover hard-coral cover, guild fractions, substrate classes and a condition index on held-out sites, years and reefs, with skill surviving depth stratification, spatial buffering, and transfer across programmes and eras. In the *change regime*, the same embedding supports year-over-year inference only when an acute event intervenes, and only at 20–50 m aggregation; quiet-year benthic change sits below the noise floor of the registered linear protocol at every scale tested, the read-out's limit rather than the ground truth's (§3.5). The implied instrument is an annual reef-state mapper with an event-triggered change detector, not a continuous change monitor.

The regime boundary has a physical reading, offered as the most parsimonious interpretation, with one source caveat: the embedding also ingests non-optical sensors (§2.2) and per-sensor attribution is beyond what a decodability survey can establish, so "optical character" below means the persistent multi-sensor signature of the pixel. An annual embedding averages a year of observation, so it measures the persistent state of a pixel well and its within-year trajectory poorly; slow compositional drift (a few points of cover per year) is smaller than the year-to-year noise of the composite, while an event-scale substrate conversion (live coral to standing dead structure to turf) changes the persistent optical character of the pixel and is readable.

Consistent with this, the signed change decoders behave as substrate-conversion detectors: they read the loss direction well, tracking realised cover loss rather than whitening (§3.3); they read rebound-year regrowth with inverted sign; and they find nothing in the two transitions where no conversion occurred.

The same persistence logic offers a reading of the substrate channels. Standing-dead coral and rubble are both EAM-covered surfaces and should be near-identical spectrally at 10 m through a water column, yet standing-dead transfers across reefs unconditionally while rubble does not. The candidate carrier is structural persistence: standing dead colonies keep their arrangement in place across a compositing year, whereas rubble is mobile fragments whose configuration changes within it. Neither channel is a live-coral inverse (§3.1); the persistence reading is consistent with the transfer pattern but not a demonstrated mechanism.

A revision-round probe adds a consistent optical signature: within-year Sentinel-2 scene-to-scene variability is higher where the substrate mix tilts toward rubble, and across all pixel-years instability tracks the mobile substrates while the fixed ones sit at or below zero. This is supportive but confounded with wave exposure, so the reading remains an interpretation (numbers in supplement §S6, r45).

The post-registration campaign (§3.7) adds a third behaviour: a succession artifact, defined operationally as a look-alike residual: given true cover, the coral decoder over-predicts where turf-covered standing skeleton is present, so decoded trajectories run optimistic after loss and rank true gains below chance at never-trained reefs. The persistence logic explains it: algal turf recolonises standing structure within a compositing year, restoring a coral-like optical character long before the ecology recovers. The campaign also decomposes the quiet-year noise by scale: within a reef, a fresh spatially smooth error field each year that no static map can correct; between years, a per-year whole-window offset that dominates reef-mean noise away from the training reef (§3.7).

4.2 Implications for monitoring programmes

For a monitoring programme, the catalogue translates into a concrete set of map products: a 10 m drill-down tier (meso-scale caveat), a 50 m primary mapping tier, and 100 m regional roll-ups for state (sparse-aggregate caveat, §3.4); a 20–50 m event-response tier for change. The state tiers should be read for what the persistence control (§3.1) shows they are: maps of largely static habitat structure, annually re-observed, whose value is coverage and consistency rather than year-to-year sensitivity; year-specific information enters through the event tier.

Two extension properties were measured, and each must be quoted as the quantity its test actually measured. First, cross-reef transfer is real but is mostly reef ranking, and the pixel-level number to quote is the reef-identity floor (§3.1): within a never-trained reef, a decoder trained elsewhere ranks pixels at roughly half the within-programme skill for the strong channels, less for the guilds. What this supports is extending state maps from a programme's surveyed reefs to unsurveyed shallow-reef habitat *of the kinds the transfer tests actually sampled* (habitat-mapping campaign reefs along one south-to-north, cross-programme axis; §2.1), with disclosed skill loss and periodic recalibration. Off the training programme the state product is a ranking instrument (absolute calibration does not transfer; §3.7), but the ranking adds information over a static habitat map, and the envelope is measured: to ~9 m depth (91.6 % of GBR10 Coral/Algae pixels lie at 0–9 m), across regional holdouts, and with all training reefs 200 km away.

Recalibration is measured, not assumed: deployed to the 38 never-trained survey tables with its threshold fixed from Heron, the worst-quartile alarm's false-positive rate drifts and its detection is not separable from chance, while label-free per-reef recalibration restores the 10 % budget (§3.3; supplement §S6, r44). It does not support mapping without ground truth: the conditional channels need exactly the local field data that skipping ground truth would save, and every validated claim remains bounded to ground-truthed reefs.

Second, the event-response tier is a ranked triage map from the coral-loss axis (§4.1): once the annual layer covering a thermal-stress year is released, the axis ranks ≥ 10-point loss blocks at 20 m (AUC .83 in 2024, .66 in 2020), with detection estimable only to the wide interval in §3.3. Alarm thresholds do not transfer between events, so the deliverable is a ranking within the new layer rather than a fixed alarm; rebound-year layers must not be run through the loss axis at all (it reads first-year regrowth as anti-loss; §3.3). Three campaign bounds refine the tier (§3.7): the axis outperforms plain differencing; it tracks the thermal-stress gradient in moderate years but saturates in a severe one, where it flags without ranking; and post-event windows decay within about a year, so detection has a one-year shelf life. Its ground-truth budget is bound by site diversity rather than image count (§S13).

The increment over existing products: thermal-stress products already name the event and its exposure footprint; the triage map adds a spatially complete 20 m coral-loss *ranking* within that footprint (subject to the same transfer bounds; validated at the one reef with change ground truth). Annual layers publish months after the composite year closes, so the niche is planning the following field season, not rapid response. In the four non-event transitions the product returns no detections, as intended. Both validated events are thermal; cyclone- and predation-driven loss remain untested (§3.7).

Aggregation adds one bounded change capability at calibrated reefs (§3.7): the reef-mean index resolves a change of about 7 true points of coral cover (14 at site scale) at any speed, so a slow decline becomes visible once it crosses the floor (§3.7). At never-trained windows the per-year offset raises that floor roughly five-fold, so reef-mean change tracking requires local calibration, and apparent gains are distrusted wherever the succession artifact is uncorrected (§4.1).

The conditionality results are as operationally important as the skills. Rubble maps do not transfer beyond the training reef (the prevalence-conditioned lead is held in the supplement pending confirmation); macroalgae maps are valid only where macroalgae is abundant (carried entirely by one survey programme, region and year; §3.5); and no quiet-year change product should be issued at any scale. These conditions require local ground truth to evaluate: a programme adopting embedding-based mapping needs the catalogue's conditions, not just its headline correlations.

4.3 Complementarity with existing approaches

The embedding approach neither replaces optical mapping nor in-water monitoring; it sits between them. Relative to the Allen Coral Atlas, the embedding reproduces the Atlas's classes (AUC .87–.97) and adds what a static map cannot: annual revisit, continuous guild-level cover channels, and event response. Both halves are now measured externally (§3.7): decoded sand reproduces the Atlas at all seven tested never-trained reefs, and the annual index predicts external coral cover where a static habitat-class fraction carries none. Relative to plain optical time series, the appropriate comparison is the ablation (§3.1): the embedding adds measured skill over plain, multi-temporal and red-edge/SWIR-widened Sentinel-2 baselines on every catalogue channel except sand (and rubble against the widened baseline only).

The Sentinel-1-alone baseline closes the radar side of the attribution question (§3.1): the measured increment is carried by something beyond both plain optics and radar, and the embedding's multi-sensor temporal integration remains the simplest reading. Claims of the form "only embeddings can do this" are not supported; the supported claim is the measured increment.

Relative to in-water programmes, the dependence runs the other way: every decoded channel exists only because photo-quadrat ground truth trained it, and the ceiling analysis shows the binding constraints are signal physics and ground-truth reliability, not model capacity or sample size. Embedding-based mapping is a multiplier on field programmes, not a substitute, and archived photo-quadrat data gains new value as training data.

4.4 Decoder capacity and the skill ceiling

Ridge regressions on 64 features were sufficient throughout, and three results argue this is not a modelling shortfall. Learning curves plateau by a quarter of the available training data for every channel, so capacity is not data-starved; the nonlinear gain is real but small and already quantified (§3.1); and the measured ground-truth reliability places the ceiling at rho ≈ .7–.8 for the strongest channels (§3.1), so held-out skill is already near what noise-free ground truth would permit. The unexplained remainder is attributable to sub-pixel benthic mixing, water-column variation and whatever the embedding compression discarded.

The campaign adds the analogous external benchmark (§3.7): two independent survey programmes agree at only rho .71 on cover levels, and external skill is roughly a third of that agreement at site grain, a quarter at manta-window grain. The trajectory failures have no such excuse: the same programmes agree with each other on year-to-year change where the index reads nothing. The residual transfer loss has survived an elimination battery (§3.7); it behaves like, though is not proven to be, a physical limit.

4.5 Methodological results that generalise

Three findings apply beyond reefs, to any pairing of learned satellite representations with field ecology. (i) Spatial leakage is not a technicality: a naive random-pixel split inflated skill by +.10–.28 rho on identical data and models, replicated on the independent cross-reef set (§3.5); studies reporting embedding decodability under random splits are reporting leakage. (ii) Annotation schemes are a first-class variable: pooling ground truth across two annotation programmes inflated substrate-channel skill through pure source contrast (§3.5), and systematic annotation error destroyed the *Acropora*-complex channel on one CoralNet export while leaving total-cover channels intact (§3.5); decoding studies should treat ground-truth source like site, as a clustering unit to demean and hold out. (iii) Clustered inference changes conclusions: several channels significant under naive p-values fail under site- or reef-cluster bootstrap; every number in this catalogue carries clustered uncertainty. (iv) Trajectories from state indices need change-side validation: decoded state read-outs were directionally biased on post-disturbance reefs at every external grain tested here, consistent with succession restoring a surface's optical character before its ecology (§3.7); any satellite index of ecosystem state should be screened for this artifact class before its trends are interpreted.

4.6 Limits and the data that resolve them

The post-registration campaign resolved several items this section originally left to future data, mostly against the catalogue. Cross-reef change replication was run on the archives that held it and failed with a measured directional bias (the succession artifact, §4.1) rather than for lack of data (§3.7). Recovery detection is externally invalidated in the gain direction; what it needs is a succession-robust feature that separates turf-covered skeleton from live coral more sharply than any current channel. Pressure attribution moved partway: the loss-axis footprint tracks thermal forcing in moderate years and saturates in severe ones, while cyclone response stays untested (§3.7).

The items that remain open are fewer and sharper: a second change-calibrated reef (the reef-scale detection bound is calibration-reef-scoped, and the per-year whole-window offset blocking its generalisation is measured but unexplained); a validated non-thermal event; the single-campaign macroalgae conditional and the rubble prevalence lead (unchanged); and the loss-side external lead (a succession-corrected composite reaching AUC .635 at never-trained sites) awaiting registered confirmation. The survey design of registered predictions, one protocol and reported negatives is intended to be rerun as that ground truth and each annual embedding layer arrives.

4.7 Conclusions

A global, general-purpose annual satellite embedding, read with linear decoders against photo-quadrat ground truth, supports a validated catalogue of shallow-reef information (eight benthic state channels across 10–100 m scales, event-gated loss detection at 20–50 m validated at one reef, two near-ceiling auxiliary layers, and a demonstrated separation of gaining from losing reef in event years), together with sharply mapped limits, several of which are the study's own controls: state skill is dominated by persistent habitat structure, cross-reef pixel skill is roughly half the within-programme number, and quiet-year change is undetectable by the registered linear read-out. A post-registration campaign against independent monitoring archives sharpened both edges: state levels transfer (at a quarter to a third of the measured inter-programme agreement, depending on grain), trajectories fail with a measured directional bias (the succession artifact), and reef-mean aggregation resolves ≈ 7-point changes only at locally calibrated reefs (§3.7).

For reef monitoring the practical meaning is bounded: within surveyed reefs, decoding runs near the ground-truth ceiling; on never-trained reefs it drops to the reef-floor numbers and is a ranking rather than a calibrated measure; in event years a change ranking exists at one validated reef; and every tier remains anchored to the field programmes whose archives train it. For remote sensing, the meaning is that embedding fields carry usable marine information they were not built to expose (more than plain optical baselines on most channels, though not all), and that extracting it reliably requires the effort to go into validation rather than model complexity.

Declarations and acknowledgments

Acknowledgments

This work rests on the field programmes whose photographic archives make it possible: the University of Queensland Heron Reef monitoring programme (Golding et al., 2026; Roelfsema et al., 2021b), the UQ regional photo-transect campaigns (Roelfsema et al., 2018a–c, 2022a–b), the Reef Life Survey Foundation and its volunteer divers, and the Australian Institute of Marine Science.

As this was a desk-based study of archived data held by custodial monitoring programmes, with no new data collection, no Indigenous consultation was sought.

Prescribed data-custodian texts: The AlphaEarth Foundations Satellite Embedding dataset is produced by Google and Google DeepMind. Contains modified Copernicus Sentinel data [2017–2025]. Degree Heating Week data were provided by NOAA Coral Reef Watch. Allen Coral Atlas maps, bathymetry and map statistics are © 2018–2023 Allen Coral Atlas Partnership and Arizona State University and licensed CC BY 4.0. The eReefs datasets (model simulations, satellite or in-situ observations; Baird et al., 2020) and software were produced as part of the eReefs project (ereefs.org.au), which is a collaboration between Australia's national science agency CSIRO, the Australian Institute of Marine Science (AIMS) and the Queensland Government, with observations obtained through the Integrated Marine Observing System (IMOS) and the Great Barrier Reef Marine Park Authority (GBRMPA). eReefs is funded by the Australian Government's Reef Trust.

Funding

This research was supported by the Commonwealth through an Australian Government Research Training Program Scholarship [DOI: https://doi.org/10.82133/C42F-K220]. The candidature is undertaken through the James Cook University PhD@Work program, hosted at OSIBOT PTY LTD; no other project-specific funding was received. The funding sources had no role in study design; collection, analysis and interpretation of data; writing of the report; or the decision to submit the article for publication.

Data availability

All inputs are public except the Heron Island ReefCloud photo-quadrat summaries (available on request from the custodian). The released pack reproduces the fully public tier end-to-end; the Heron tables additionally require the custodian data. The AlphaEarth embedding windows used are archived at https://doi.org/10.5281/zenodo.22065348 under the dataset's CC-BY 4.0 licence, and trained decoder coefficients are released with the pack (§2.10). Full source and licence tables: `../DATA-AVAILABILITY.md`.

Code availability

The public reproduction pack (companion analysis library, per-run scripts, and the run ledger) is released at https://doi.org/10.5281/zenodo.22065301; the scripts acquire the public datasets directly from their sources. The supplementary material is deposited at https://doi.org/10.5281/zenodo.22064963.

Author contributions (CRediT)

A.C.: conceptualisation, data curation, formal analysis, investigation, methodology, software, validation, visualisation, writing — original draft, writing — review and editing.

Declaration of competing interest

The author is founder and director of OSIBOT PTY LTD, a marine robotics and survey company that hosts the author's PhD@Work candidature and in which intellectual property arising from the candidature vests. OSIBOT has no commercial product based on the methods evaluated here. The author declares no other competing interests.

Ethics and permits

Field data were collected by the custodial programmes under their own permits and approvals; this study analyses archived data held by custodial monitoring programmes (publicly available or available on request) and involved no new field collection. No human-participant or animal research was undertaken and no ethics approval was required.

Declaration of AI and AI-assisted technologies in the writing process

During the preparation of this work the author used Cursor, with the Fable 5 and Grok 4.6 AI models, in order to assist in drafting the manuscript. After using these tools, the author reviewed and edited the content as needed and takes full responsibility for the content of the publication.

References

Cited works

- AIMS (2025). *Annual Summary Report of Coral Reef Condition 2024/25.* Australian Institute of Marine Science, Townsville.
- Baird, M.E., Wild-Allen, K.A., Parslow, J., et al. (2020). CSIRO Environmental Modelling Suite (EMS): scientific description of the optical and biogeochemical models (vB3p0). *Geoscientific Model Development* 13, 4503–4553.
- Beijbom, O., Edmunds, P.J., Roelfsema, C.M., Smith, J.E., Kline, D.I., Neal, B.P., Dunlap, M.J., Moriarty, V., Fan, T.-Y., Tan, C.-J., Chan, S., Treibitz, T., Gamst, A., Mitchell, B.G., Kriegman, D. (2015). Towards automated annotation of benthic survey images: variability of human experts and operational modes of automation. *PLoS ONE* 10(7), e0130312.
- Brown, C.F., Kazmierski, M.R., Pasquarella, V.J., et al. (2025). AlphaEarth Foundations: an embedding field model for accurate and efficient global mapping from sparse label data. *arXiv* 2507.22291.
- Byrne, M., Waller, A., Clements, M., et al. (2025). Catastrophic bleaching in protected reefs of the Southern Great Barrier Reef. *Limnology and Oceanography Letters* 10, 340–348.
- Ceccarelli, D.M., Emslie, M.J., Logan, M., et al. (2026). Substantial impacts from the 2024 summer reverse five years of coral cover gains on the Great Barrier Reef. *Coral Reefs*, doi:10.1007/s00338-026-02829-8.
- Courtney, J.B., Foley, G.R., van Burgel, J.L., Trewin, B., Burton, A., Callaghan, J., Davidson, N.E. (2021). Revisions to the Australian tropical cyclone best track database. *Journal of Southern Hemisphere Earth Systems Science* 71, 203–227.
- Diederiks, F.F., Hammerman, N.M., Staples, T., Kovacs, E., Markey, K., Roelfsema, C.M. (2025). Remote sensing reveals multidecadal trends in coral cover at Heron Reef, Australia. *Remote Sensing* 17(7), 1286.
- Edgar, G.J., Cooper, A., Baker, S.C., et al. (2020). Establishing the ecological basis for conservation of shallow marine life using Reef Life Survey. *Biological Conservation* 252, 108855.
- Edgar, G.J., Stuart-Smith, R.D. (2014). Systematic global assessment of reef fish communities by the Reef Life Survey program. *Scientific Data* 1, 140007.
- Friedman, A., Monk, J., Pizarro, O., Lindsay, D., Oh, E., Thornton, B., Carroll, A., Przeslawski, R., Williams, S. (2026). Squidle+: a collaborative platform to manage, discover and annotate marine imagery. *Frontiers in Marine Science* 12, 1677103.

- Golding, K., Smart, J., Cowley, D., Carrasco Rivera, D.E., Hammerman, N., Markey, K., Kovacs, E., Diederiks, F., Passenger, J., Roelfsema, C. (2026). Georeferenced benthic photo quadrats and benthic cover data derived from a time series of transect surveys for Heron Reef flat and slope areas, Great Barrier Reef, 2019–2025. University of Queensland Research Data Manager, doi:10.48610/7df1430.
- González-Rivero, M., et al. (2020). Monitoring of coral reefs using artificial intelligence: a feasible and cost-effective approach. *Remote Sensing* 12(3), 489.
- Hedley, J.D., et al. (2016). Remote sensing of coral reefs for monitoring and management: a review. *Remote Sensing* 8(2), 118.
- Hedley, J.D., Roelfsema, C., Brando, V., et al. (2018). Coral reef applications of Sentinel-2: coverage, characteristics, bathymetry and benthic mapping with comparison to Landsat 8. *Remote Sensing of Environment* 216, 598–614.
- Hochberg, E.J., Atkinson, M.J. (2003). Capabilities of remote sensors to classify coral, algae, and sand as pure and mixed spectra. *Remote Sensing of Environment* 85, 174–189.
- Hughes, T.P., et al. (2017). Global warming and recurrent mass bleaching of corals. *Nature* 543, 373–377.
- Hughes, T.P., et al. (2018). Spatial and temporal patterns of mass bleaching of corals in the Anthropocene. *Science* 359, 80–83.
- Kennedy, E.V., Roelfsema, C.M., Lyons, M.B., et al. (2021). Reef Cover, a coral reef classification for global habitat mapping from remote sensing. *Scientific Data* 8, 196.
- Liu, G., Heron, S.F., Eakin, C.M., et al. (2014). Reef-scale thermal stress monitoring of coral ecosystems: new 5-km global products from NOAA Coral Reef Watch. *Remote Sensing* 6(11), 11579–11606.
- Lyons, M.B., et al. (2020). Mapping the world’s coral reefs using a global multiscale earth observation framework. *Remote Sensing in Ecology and Conservation* 6(4), 557–568.
- Rahman, M. (2026). Physically interpretable AlphaEarth foundation model embeddings enable LLM-based land surface intelligence. *Remote Sensing Applications: Society and Environment*, doi:10.1016/j.rsase.2026.102045.
- Roelfsema, C.M., Lyons, M.B., Castro-Sanguino, C., et al. (2021a). How much shallow coral habitat is there on the Great Barrier Reef? *Remote Sensing* 13(21), 4343.
- Roelfsema, C., Kovacs, E.M., Vercelloni, J., et al. (2021b). Fine-scale time series surveys reveal new insights into spatio-temporal trends in coral cover (2002–2018), of a coral reef on the Southern Great Barrier Reef. *Coral Reefs* 40, 1055–1067.
- Skirving, W., Marsh, B., De La Cour, J., et al. (2020). CoralTemp and the Coral Reef Watch coral bleaching heat stress product suite version 3.1. *Remote Sensing* 12(23), 3856.

- Sweatman, H., Delean, S., Syms, C. (2011). Assessing loss of coral cover on Australia's Great Barrier Reef over two decades, with implications for longer-term trends. *Coral Reefs* 30(2), 521–531.
- Yamano, H., Tamura, M. (2004). Detection limits of coral reef bleaching by satellite remote sensing: simulation and data analysis. *Remote Sensing of Environment* 90(1), 86–103.

Dataset and platform citations

- Allen Coral Atlas (2022). Imagery, maps and monitoring of the world's tropical coral reefs. Zenodo, doi:10.5281/zenodo.3833242.
- Australian Institute of Marine Science (AIMS) (2017). AIMS Long-Term Monitoring Program: Crown-of-Thorns Starfish (*Acanthaster planci*) and Benthos Manta Tow Data (Great Barrier Reef). doi:10.25845/5c09b0abf315a.
- Australian Institute of Marine Science (AIMS) (2024). ReefCloud. doi:10.25845/g5gk-ty57. *(platform citation; Heron data cited as Golding et al. 2026)*
- Beaman, R.J. (2017). High-resolution depth model for the Great Barrier Reef — 30 m. Geoscience Australia, doi:10.4225/25/5a207b36022d2. *(2020-refresh grid under the same record)*
- Bureau of Meteorology (n.d.). Australian Tropical Cyclone Database. http://www.bom.gov.au/cyclone/tropical-cyclone-knowledge-centre/databases/ (accessed 2026-08-15).
- Reef Life Survey (RLS); Integrated Marine Observing System (IMOS) (2026). IMOS — National Reef Monitoring Network Sub-Facility — Global benthic cover data (photoquadrat image annotations); accessed via Squidle+ public collections (RLS GBR 2018/2019 and Coral Sea 2019 campaigns), 2026-08-15. https://metadata.imas.utas.edu.au/geonetwork/srv/api/records/0a65be6d-1c76-49ac-a151-80acf123612c.
- NOAA Coral Reef Watch (2018, updated daily). NOAA Coral Reef Watch Version 3.1 Daily Global 5km Satellite Coral Bleaching Degree Heating Week Product, 2016–2025 subset. College Park, Maryland, USA: NOAA Coral Reef Watch (accessed 2026-08-15).
- **[2018a]** Roelfsema, C.M., Kovacs, E.M., Markey, K., Phinn, S.R. (2018). Benthic and substrate cover data derived from field photo-transect surveys for the Cairns to Cooktown management region of the Great Barrier Reef (GBR), January and April/May 2017 [dataset publication series]. PANGAEA, doi:10.1594/PANGAEA.892623.
- **[2018b]** Roelfsema, C.M., Kovacs, E.M., Markey, K., Phinn, S.R. (2018). Benthic and substrate cover data derived from field photo-transect surveys for the Far Northern management region of the Great Barrier Reef [dataset publication series]. PANGAEA, doi:10.1594/PANGAEA.891736.
- **[2018c]** Roelfsema, C.M., Kovacs, E.M., Stetner, D., Phinn, S.R. (2018). Georeferenced benthic photoquadrats captured annually from 2002–2017,

distributed over Heron Reef flat and slope areas [dataset publication series]. PANGAEA, doi:10.1594/PANGAEA.894801.

- **[2022a]** Roelfsema, C.M., Kovacs, E.M., Markey, K., Phinn, S.R. (2022). Benthic and substrate cover data derived from field photo-transect surveys for the Townsville to Whitsunday management region of the Great Barrier Reef (GBR), May/June 2019 [dataset]. PANGAEA, doi:10.1594/PANGAEA.946748.
- **[2022b]** Roelfsema, C.M., Kovacs, E.M., Markey, K., Phinn, S.R. (2022). Benthic and substrate cover data derived from field photo-transect surveys for the Mackay to Capricorn management region of the Great Barrier Reef (GBR), May/June 2019 [dataset]. PANGAEA, doi:10.1594/PANGAEA.946749.

Figure captions

Figures are generated from the confirmatory run ledger or rebuilt with the published pipeline; one script per figure.

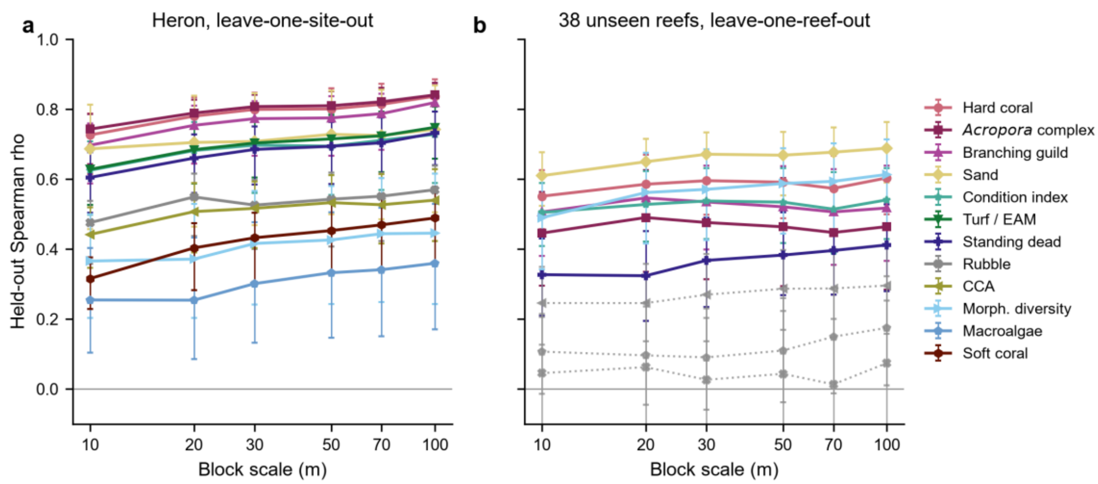

Figure 1. State-channel decodability by spatial scale (`fig01_skill_by_scale`)

Held-out Spearman rho for every evaluated state channel at 10–100 m block scales. **(a)** Heron Reef, leave-one-site-out (min. 2 images per pixel-year); whiskers are site-cluster bootstrap 95 % CIs. **(b)** The 38 genus-resolved 2017 survey tables (35 named reefs), leave-one-reef-out; whiskers are reef-cluster CIs. Dotted grey marks the two register channels not carried in the catalogue (crustose coralline algae, morph-bin entropy; §3.1). Pooled cross-reef rho includes a between-reef ranking component, decomposed in Fig. 2d. Sand is optically decodable and not primary evidence for the embedding method (Fig. 6).

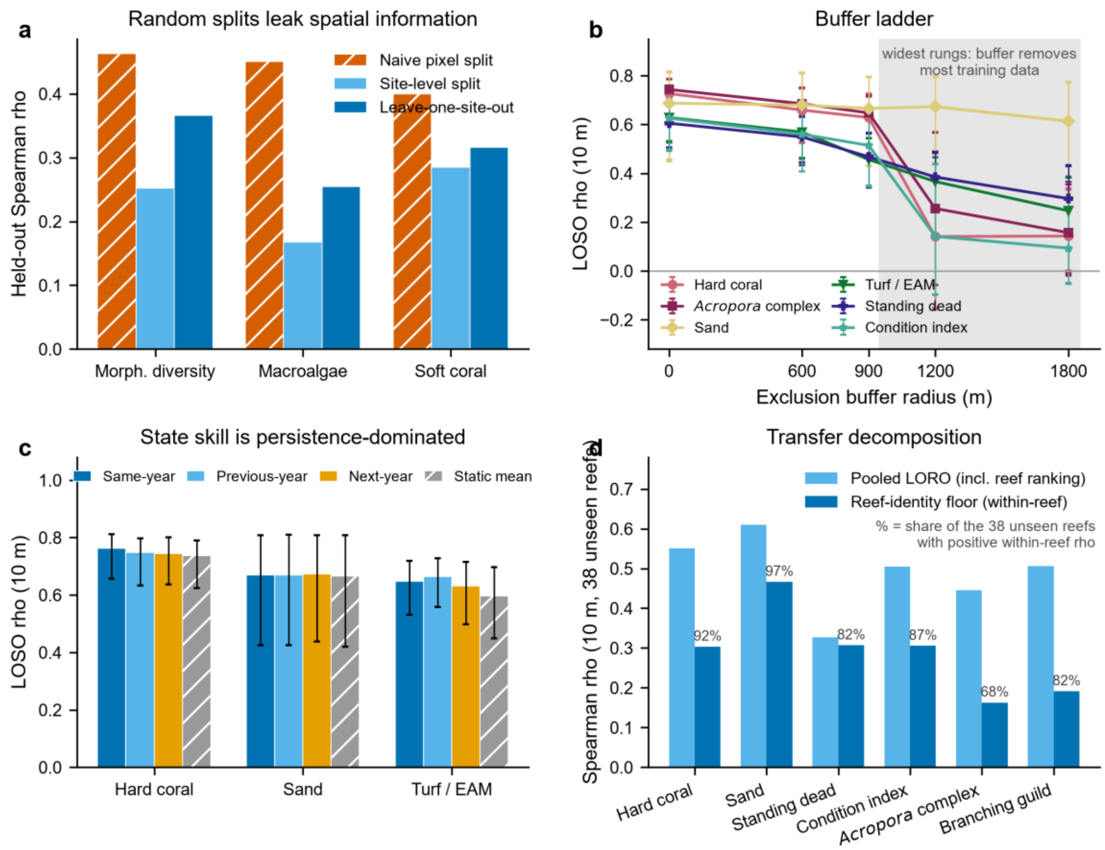

Figure 2. The validation battery (`fig02_validation_battery`)

(a) Spatial-leakage quantification: a naive random-pixel 75/25 split inflates apparent skill relative to a site-level split and leave-one-site-out on identical data and models (three channels; r10). **(b)** Buffer ladder: 10 m LOSO rho with exclusion buffers of 0–1800 m; skill is stable to 900 m; the shaded region marks the widest rungs, where the drop reflects domain truncation rather than leakage (r30). **(c)** Persistence control: replacing same-year embeddings with previous-year, next-year or static-mean embeddings barely degrades state skill (r34). **(d)** Cross-reef transfer decomposition: pooled leave-one-reef-out rho versus the reef-identity floor (median within-reef rho on never-trained reefs); percentages give the fraction of reefs with positive within-reef rho (r05).

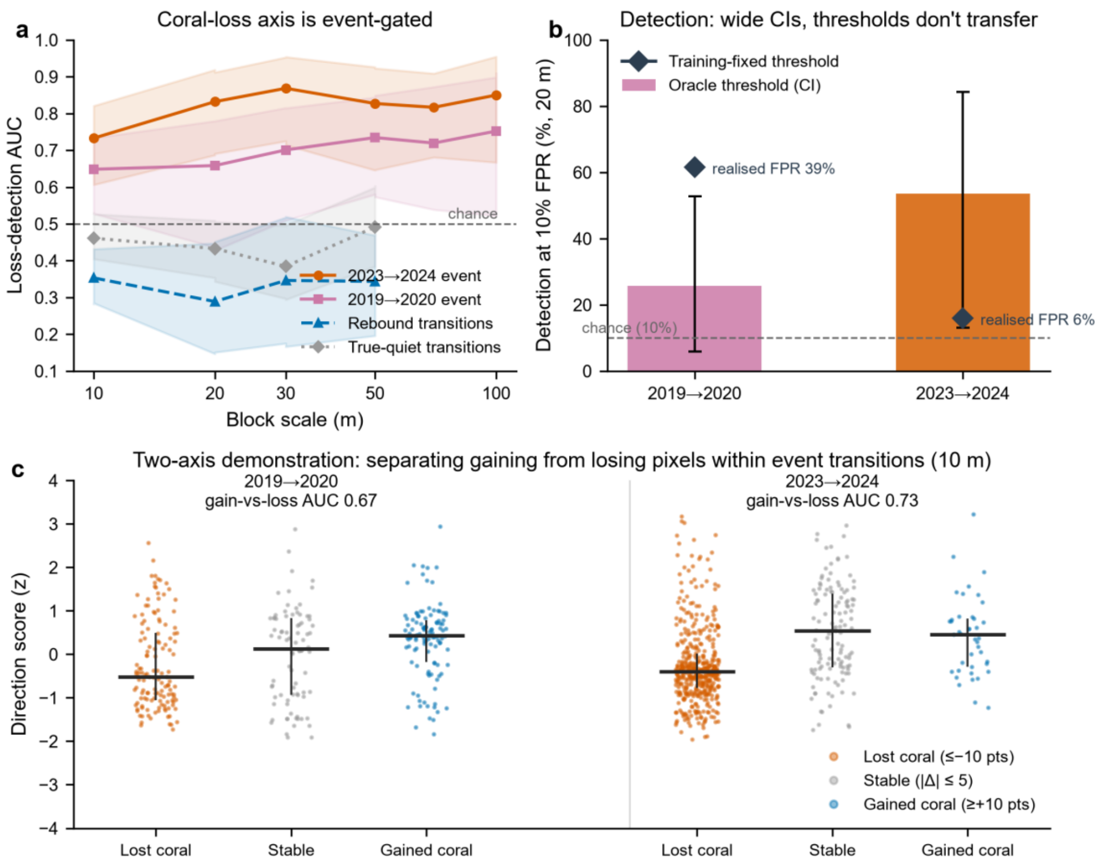

Figure 3. The change regime (`fig03_change_regime`)

(a) Coral-loss axis AUC (≥ 10-pt loss vs stable, leave-one-transition-out) by scale, split by transition class: two thermal-stress events, two rebound transitions, two true-quiet transitions; shading = cluster 95 % CIs. Rebound transitions sit below chance: the axis reads direction, not disturbance per se (r03, r27). **(b)** Detection at a 10 % false-positive budget, 20 m: oracle-threshold detection with cluster CIs, and the operating points realised when the threshold is fixed on the other event; thresholds do not transfer (r26). **(c)** Two-axis demonstration at 10 m: combined recovery+loss direction score for pixels that lost (≤ −10 pts), stayed stable (|Δ| ≤ 5) or gained (≥ +10 pts) hard coral within each event transition (axis training excludes the evaluated pair; ticks group medians, lines interquartile ranges; r09).

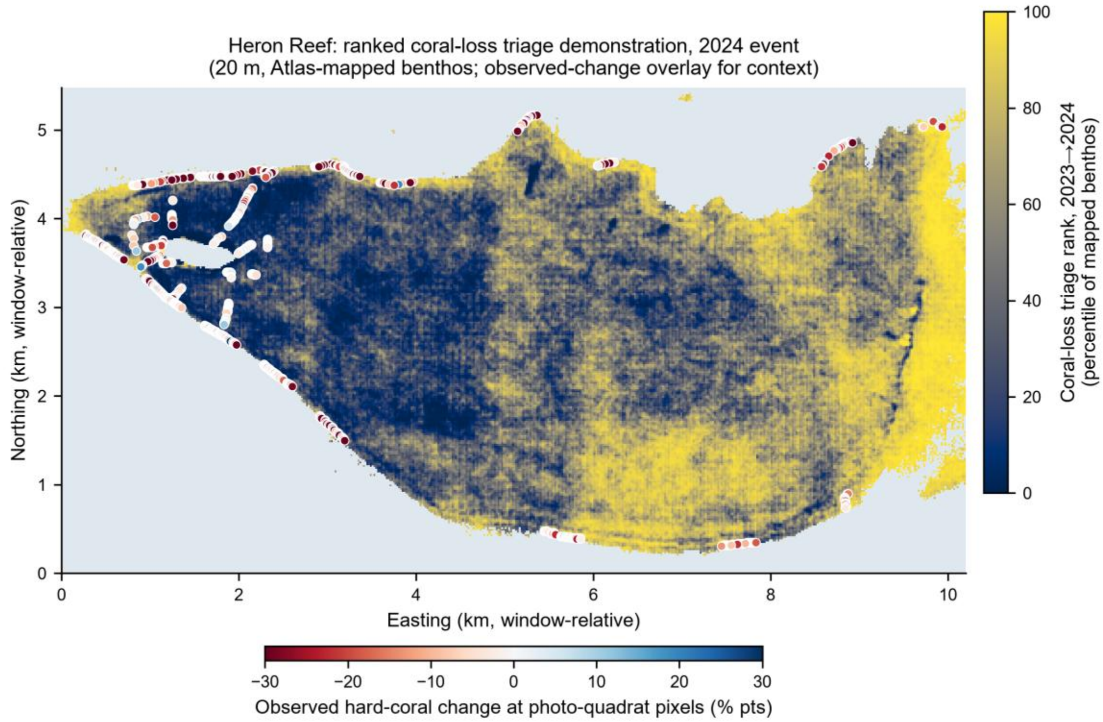

Figure 4. Ranked coral-loss triage demonstration, Heron 2024 (`fig04_loss_triage_map`)

Coral-loss axis applied to the full Heron Δ-embedding field for 2023→2024, trained only on the other transitions, aggregated to 20 m and expressed as percentile ranks over Atlas-mapped benthos (unmapped/deep water in grey-blue). Overlaid circles: ground-truth pixels coloured by observed hard-coral change (the estimands differ; context, not a validation scatter). Demonstration only: the field is demeaned over the displayed domain, whereas confirmatory metrics demean over ground-truth support (§2.7).

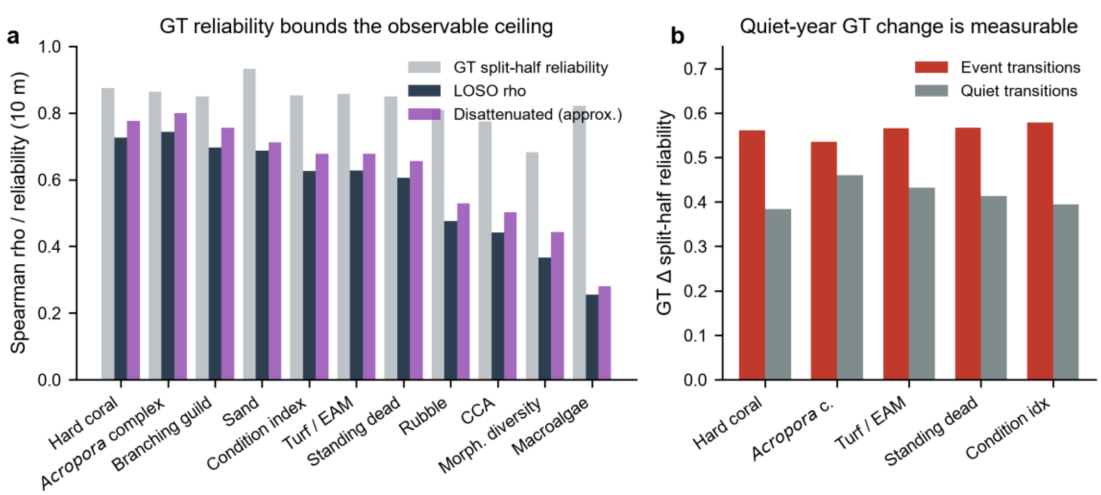

Figure 5. Ground-truth reliability and the decoding ceiling

(`fig05_reliability_ceiling`)

(a) Per channel at 10 m: ground-truth split-half reliability (Spearman–Brown), observed LOSO rho, and the disattenuated ratio rho/√reliability; the disattenuation uses a classical error model and is approximate (r13). **(b)** Split-half reliability of year-over-year ground-truth change for event vs quiet transitions: quiet-year change is measurable in the ground truth (reliability ≈ .3–.5), so the quiet-year decoding null is not a ground-truth-noise artefact (r21).

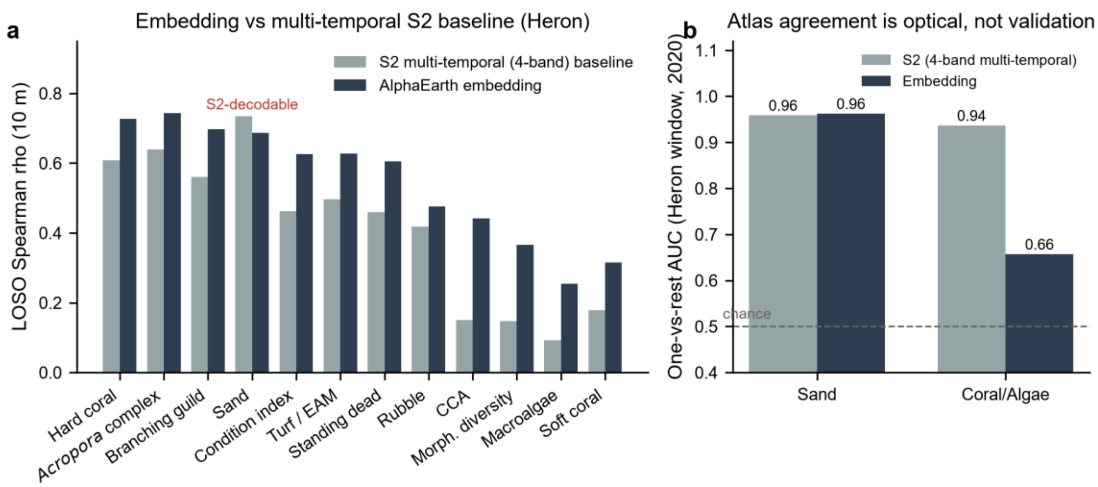

Figure 6. What the embedding adds over plain optics

(`fig06_optical_baseline`)

(a) Heron 10 m LOSO rho: the strengthened multi-temporal Sentinel-2 baseline (per-scene-normalised 10th/50th/90th percentile stack of the four 10 m bands; 12 features, ridge decoders under identical folds; §2.6) versus the embedding decoder, per channel. The embedding adds skill on every channel except sand, which plain optics slightly beats (S2 .73–.77 vs embedding .69; r23). **(b)** Allen Coral Atlas class agreement over the Heron window (2020 layer; one-vs-rest AUC, 100 m-cell cluster protocol): the Atlas is itself optically derived, so high S2 agreement is expected shared-optics circularity (Coral/Algae S2 .94 vs embedding .66; sand near-tied); Atlas agreement is not accuracy validation (r32).